
Article:
Ashworth, S. orcid.org/0000-0003-1192-6127, Fairclough, J.P.A. orcid.org/0000-0002-1675-5219, Takikawa, Y. et al. (4 more authors) (2019) Effects of machine stiffness and cutting tool design on the surface quality and flexural strength of edge trimmed carbon fibre reinforced polymers. Composites Part A: Applied Science and Manufacturing, 119. pp. 88-100. ISSN 1359-835X

https://doi.org/10.1016/j.compositesa.2019.01.019

Effects of machine stiffness and cutting tool design on the surface quality and flexural strength of edge trimmed carbon fibre reinforced polymers

Sam Ashworth, J. Patrick A. Fairclough, Yoshihiro Takikawa, Richard Scaife, Hassan Ghadbeigi, Kevin Kerrigan, James Meredith

PII: S1359-835X(19)30027-2
DOI: https://doi.org/10.1016/j.compositesa.2019.01.019
Reference: JCOMA 5314

To appear in: *Composites: Part A*

Received Date: 18 May 2018
Revised Date: 15 January 2019
Accepted Date: 23 January 2019

Please cite this article as: Ashworth, S., Patrick A. Fairclough, J., Takikawa, Y., Scaife, R., Ghadbeigi, H., Kerrigan, K., Meredith, J., Effects of machine stiffness and cutting tool design on the surface quality and flexural strength of edge trimmed carbon fibre reinforced polymers, *Composites: Part A* (2019), doi: https://doi.org/10.1016/j.compositesa.2019.01.019

Effects of machine stiffness and cutting tool design on the surface quality and flexural strength of edge trimmed carbon fibre reinforced polymers

Authors

Sam Ashworth[a,b,e], J. Patrick A. Fairclough[b], Yoshihiro Takikawa[c], Richard Scaife[d],Hassan Ghadbeigi[b], Kevin Kerrigan[d,f], James Meredith[b,f]

a - Industrial Doctorate Centre in Machining Science, Advanced Manufacturing Research Centre with Boeing, University of Sheffield, Rotherham, S60 5TZ, UK, b - Department of Mechanical Engineering, The University of Sheffield, Sir Frederick Mappin Building, Mappin Street, Sheffield, S1 3JD, UK, c - OSG Corporation,3-22 Honnogahara, Toyokawa, Aichi, 442-8543, Japan, d - Advanced Manufacturing Research Centre with Boeing, The University of Sheffield, Advanced Manufacturing Park, Wallis Way, Catcliffe, Rotherham S60 5TZ, UK, e - Corresponding author, soashworth1@sheffield.ac.uk , f - Equal contribution

Declarations of interest: None

Abstract

A 2^2 full factorial design of experiment is used to investigate the effects of two machining platforms (5-axis elevated gantry versus 6-axis articulated robotic system) and two cutting tool designs (burr versus herringbone) on surface metrics and flexural strength of a 14 ply T300 2x2 carbon fibre reinforced polymer.

A range of areal metrics were considered to characterise the surface with S_{al} and S_{tdi} best able to represent differences due to the choice of robotic system or overhead gantry. The robotic system produces coupons with flexural strengths up to 26% higher than the overhead gantry. The choice of tool has a less significant effect however machine-tool interactions do play a role in the flexural strength.

Analysis using scanning electron microscopy shows that defects may be obscured by smeared matrix which may contribute to overall flexural strength differences.

Keywords

A. Carbon Fibres, B. Defects, D. Surface Analysis, E. Machining

1. Introduction

Carbon fibre reinforced polymer (CFRP) composites are becoming more prevalent due to their superior strength-to-weight and stiffness-to-weight ratios, as aerospace [1-3] and automotive [4, 5] industries are pursuing more structurally efficient components in a drive to reduce weight and increase fuel efficiency. However, a number of issues remain in CFRP manufacturing, such as the difficulty in obtaining the required part tolerances and high cost of process consumables. The manufacturing process for CFRPs often necessitates the use of an edge trimming operation around the periphery of a net shape to achieve the final part geometry. Processes such as pre-preg layup require trimming as the bagging technique causes thickness decreases around the periphery of the laminate where the bag forces the edges to become rounded which is unwanted in the final part. In addition, the resin transfer moulding (RTM) process such as the one used in this experiment often has a fibre gap at the periphery of the press to ensure the fibres do not interrupt the mould seal in addition to loose fibres which are not consolidated and need to be removed. The surface generated through subtractive machining for CFRPs cannot be empirically determined due to the complexity of machining CFRPs and current methods rely on experimental data to provide this information. This makes linking machining to surface quality difficult and the basic relationship between the surface and the component in-service mechanical performance of the composite are not fully understood.

Typically, industry has strict tolerances for machined edge quality. For metallic parts there is a clear need for a surface roughness measurement due to the link between surface micro-defects and failure due to crack propagation [6-10]. R_a, the arithmetic mean of the micro-scale peaks and valleys of a surface (see Supplement for a full list of definitions), is most frequently used to measure such metallic surface defects [11, 12]. The same R_a measurement parameter has been used for edge trimmed CFRP parts due to availability of equipment and understanding of tribological aspects of R_a [13]. Montoya, Calamaz, Gehin and Girot [14] note that industry typically require a machined surface R_a of 3.2 µm or less for machined CFRP parts. These CFRP parts do not behave in the same way as metallic parts due to the use of two differing material phases (fibre and resin) and the combination of these in an anisotropic manner, for example in a 2x2 twill, multi-directional laminate. This fundamental material difference poses the question of whether R_a is an adequate surface measurement parameter and if it is able to correctly capture complex defects that are apparent in edge trimmed components such as aircraft engine coverings, fan blades, internal structural members and external shear panels.

Recent studies have compared the use of areal 3D versus 2D parameters and found that 3D offers more appropriate data whilst also able to fully replicate data given in 2D stylus analyses [15, 16]. The high number of parameters available makes the down-selection of a single useful metric more challenging but increases the chances of a 3D metric being able to link mechanical properties where 2D metrics have previously failed.

The effect on static or dynamic mechanical performance of an edge trimmed composite has not been fully explored due to the assumption that composites are able to arrest any crack growth and links of either R_a or another surface metric to mechanical properties are not fully understood [17]. In one of the few studies to link mechanical performance to surface metrics, Arola and Ramulu [18] performed four point bend testing for abrasive waterjet, diamond disc and PCD edge milled CFRPs in a $[(0/90/45/-45)2(0/90)]_s$ lay-up and found that no bulk strength difference was apparent. However, the data presented in this study does show a difference in peak load obtained during bend testing. A later study by Arola and Ramulu [19] notes that machining defects are a cause of differing mechanical performance with -45° plies being the point of failure within a laminate when flexurally loaded. These and other studies [20-24] all note that R_a does not fully characterise the machined edge which offers a significant opportunity for further assessment using 3D areal methods to determine if a link between surface tolerance and mechanical property can be made.

Generating different surfaces in terms of R_a has been previously completed using different tool geometries [25-30] with most tools having simple geometries such as orthogonal or single helix angles compared to available products and those used in industry. The herringbone design is intended to direct cutting forces to the centre of the composite instead of directing it towards a single edge which can cause significant delamination of the top plies of the laminate [31, 32]. Burr style tools are also being introduced to reduce cutting forces and improve feed rates, particularly during roughing operations. This experiment will use the complex herringbone and burr tool geometries to present more industrially relevant cutting forces compared to orthogonal milling trials and therefore more industrially relevant surfaces.

As more industrially relevant tooling is being considered, it is also necessary to consider more industrially relevant machines. If modern robotic machining is to be considered as a replacement for traditional elevated gantry style milling machines, there is a clear need to understand the differences between the surface tolerances achieved using both methods, and more fundamentally, any

differences in mechanical performance of the machined product. Whilst some work has been conducted to investigate dimensional errors when machining with robotic machines [33, 34], Slamani, Gauthier and Chatelain [35] are the only authors to specifically address the effect of surface roughness when comparing surfaces generated from robotic and gantry style machining, noting that R_a surface roughness did not differ between machines. The study did not extend to using 3D surface parameters which may provide additional information for edge trimmed CFRPs nor assess the effects on mechanical performance.

This paper presents an observation of the effect of two different machines and tools on a range of surface metrics which are measured through focus variation and scanning electron microscopy (SEM) to observe both surface and sub-surface defects. The edge milled samples are flexurally tested using a four point bending rig to observe links between machine stability, tool geometry and hence surface metrics on flexural strength.

2. Method

2.1. CFRP panel manufacture and characterisation

Four, 300 x 300 x 3 mm CFRP panels were manufactured by a Hypaject Mk I RTM system with diglycidyl-ether-of-bisphenol-F (DGEBF) PY306 epoxy (Huntsman, UK), triethylenetetramine (TETA) hardener (Sigma Aldrich, UK) and T300, 2x2 twill, 200gsm, TC3091000 fibres (Sigmatex, UK). The DGEBF and TETA were mixed at the specified stoichiometric ratio of 100 parts epoxy to 15 parts hardener by mass. 14 plies were stacked symmetrically about the mid-plane in a balanced manner to give $[((0,90)/(+45,-45))_3/(0,90)]s$. This lay-up was chosen to provide quasi-isotropic strength properties. The RTM mould was coated with 227CE release agent (Marbocoat, UK).

Mixed resin was drawn into the RTM machine and left under vacuum for 5 minutes to remove air from the mixture. The RTM tool was then injected at 2 bar for 30 minutes, 4 bar for 10 minutes, 5 bar for 10 minutes and 6 bar for 5 minutes. Panels were cured for 2 hours in the mould tool at 60°C and then post cured for 2 hours at 130°C following removal from the mould (± 1 °C error). All curing used a ramp rate of 2 °C/min.

Following cure, the CFRP panels were machined into snapshot coupons using an Erbauer diamond disc tile saw. These snapshot coupons were then loaded into the edge trimming fixture using a randomisation process generated via Minitab from a design of experiment (DOE) where machine and tool were set as two-level factors as per Table 1. Eight replicates per machine and tool

combination were used within this study with the exception of the ABB, DIA-HBC4 combination where 9 replicates were used.

Heslehurst [36] notes that most defects present in composite components appear during the manufacturing stage and that any defect starting from material processing will affect the long term mechanical performance of the part. In an effort to minimise variables during manufacture, the glass transition temperature (Tg), degree of cure, fibre, resin and void content were all measured. This also ensures that differences between manufactured panels are known to be at a minimum level.

A Perkin Elmer Diamond DSC was used to calculate Δh values of each manufactured panel to define degree of cure for the resin system. This ensures that the same amount of resin/hardener cross-linking has occurred between each manufactured panel which may ultimately effect the strength of the material. The resin samples were heated from 30 °C to 300 °C at 10 °C/min and then cooled at the same rate. The cycle was repeated to ensure full cure.

A Perkin Elmer DMA800 machine was used to conduct DMA analysis and provide a tan δ derived Tg for each of the three panels. Ensuring a low level of Tg variation across panels is important as temperature is known to have an effect on machining properties as noted by Kerrigan and O'Donnell [37]. Potentially lower Tg's may allow more matrix smearing and change cutting forces. A three point bend test utilising a free length of 17.5 mm and a width of 5 mm was completed to a maximum temperature of 160 °C at a ramp rate of 2 °C/min at a frequency of 1 Hz.

A single section from each panel was collected to determine fibre, resin and void volume prior to machining and to ensure similar content across all panels. The samples were mounted in Epocolor resin (Buehler, UK). Samples were polished using a Buehler Automet to the schedule defined in Ashworth, Rongong, Wilson and Meredith [38]. Inspection was performed using a Qioptiq Fusion optical system with a 5 MP Paxcam camera and Pax-it software to determine fibre, resin and void content through contrast analysis of five areas of the sample to give a full thickness account of content.

2.2. Milling equipment

The 2^2 full factorial DOE, as shown in Table 1, utilises 'machine' as a variable with two levels; the MAG Cincinnati FTV5, an overhead gantry style 5-axis milling machine and a floor-mounted ABB IRB6660–205/3.1 6-axis robotic system with an adapted spindle referred to as FTV and ABB respectively henceforth shown in Figure 1.

The FTV uses a HSK63A spindle with a Sandvik Coromant 392.41014-63 40 120B tool holder with tool extender and an ER collet. The ABB uses a HSK-50E spindle type with a Nikken HSK50E-SK16C-120P tool holder and an SK16-6A collet. Milling with both machines was completed using conventional milling with parameters recommended as per manufacturer's instructions given in Table 2 without coolant and a Karcher 001 NT 35/1 Tact Te H extraction system to remove hazardous dust with the extraction nozzle placed locally to capture chip ejection. In order to generate defects the manufacturers recommended cutting speed of 100-180 m/min was significantly exceeded.

2.2.1.Milling machine characterisation

Static modal tap tests were performed to assess and compare the stability of the FTV and ABB machines. A Kistler 8778A500 accelerometer with a sensitivity of 10.390 mV/g was positioned at the tip of the tool and a steel tipped Kistler 9726A5000 impulse force hammer with a sensitivity of 1.125 mV/N was used to strike the tool. A National Instruments NI 9234 data acquisition device (DAQ) recorded the input voltages from the accelerometer and impact hammer. MalTf software was used to process results and create magnitude versus frequency plots to show the differences in machine stiffness. Coherence of 0.8 - 1.0 was obtained for all readings to ensure reliable results, where a value of 1 indicates the input (hammer) and output (accelerometer value) is unified.

2.2.2.Milling tools

The DOE as shown in Table 1, uses tool as a factor with two factor levels; DIA-BNC (burr style) and DIA-HBC4 (herringbone style) diamond coated carbide tools (OSG Corporation, UK). DIA-BNC is a fine nicked router designed for CFRP trimming with the nick and flute form designed to eliminate uncut fibres and delamination. The DIA-HBC4 is a herringbone style router designed for high feed rates and excellent surface finishes and features a compression cutting mechanism, which neutralises cutting forces in the z axis (the length of the tool) to prevent delamination on both top and bottom laminates. The DIA-BNC tool is aimed at roughing operations where high removal rates are required whilst the DIA-HBC4 tool is aimed at finishing. Details of the geometry of the tools used for full slot milling are given in Table 3. A new tool was used for each machine and in addition, the tools were changed after 1.5 m of machining to minimise the effects of tool wear. Whilst 1.5m is well within recommended tool change interval of 60m recommended by the manufacturer [39], the effects of tool wear have been assessed through ANOVA where cumulative cutting distance (a measurement of the linear distance traversed by the tool) is measured against responses ranging from flexural strength

and S_a to all other surface metrics used within this experiment. All p-values from this study showed no statistical correlation (p-value > 0.05) to cumulative distance travelled by the tool and hence tool wear can be deemed as not a factor within this study.

The herringbone helix intersection, 6mm from the tool tip, was set to the mid-point of the CFRP coupons whilst the burr style was set to cut the CFRP 4mm upwards from the tip of the tool.

2.2.3.Milling fixture

A toggle clamp fixture, each with a 300N vertical force loading limit, was used to secure snapshot coupons for edge trimming as shown in Figure 2. Two spacers were used to move the snapshot coupon into an overhanging position for both edges and to prevent motion in the y-direction. A CFRP pad was used between the clamp and the snapshot coupon to distribute the local clamp force, preventing coupon motion in the z-direction close to the overhang zone. Movement in the x-direction is limited by the use of two sliding clamps attached to the fixture by M4 bolts. A dial test indicator gauge was used to ensure squareness in the direction of cutting during setup. Following trimming of one side, the coupon was removed, rotated by 180° and the second edge trimmed.

2.2.4.Dynamometer

To validate spindle speed, feed rate and to calculate a total power value for each machining operation, a Kistler 9139AA dynamometer was used to collect force data in the x, y and z direction (see Figure 2). The dynamometer was set to a sampling rate of 20 kHz and a 0-1 kN measuring range. The dynamometer was connected to a Kistler 5070A12100 8 channel charge amplifier and DAQ system. A rigid setup was created by using the fixture clamps to hold the workpiece whilst the fixture was attached to the dynamometer by four M10 bolts. The dynamometer in turn was rigidly clamped to the t-slot bed of the milling machines. Matlab post-processing was used to compensate for dynamometer load cell drift during post-processing.

Typically cutting/radial and tangential forces can be calculated. For composites this is more complex, especially for multi-directional laminates and complex tool geometries with dual and opposing helixes due to the need to calculate specific cutting energy coefficients through experiment for each of the plies and use mechanistic models to summate these forces [40]. The use of radial or tangential forces does not include z force components (along the length of the tool) which are also a significant factor when using tools with helix angles which direct forces into the tool axis. An alternative used within this experiment to allow for comparison of machines and tools is to calculate a

total power value for each cut. This takes the raw force data in the x, y and z direction from the dynamometer from start to the end of the cut. A specific algebraic sum of forces (Nm) is calculated as the integral of force as a function of distance cut within Matlab. This is then divided by the total volume of material removed to provide the total power of the tool and workpiece interaction, U_T (N/mm^2). Using this method also has the added advantage of accounting for slight thickness variations found in the samples (3.4 ± 0.2 mm) as well as capturing heat elements of work which would otherwise not be possible. Whilst a dial test indicator (DTI) has been used to align the cutting edge with the cutting axis of the machine, DTI error may result in small amounts of cross-talk in the x and y channels of the dynamometer. By capturing all the forces, any cross-talk due outstanding minor alignment issues can be ignored. The total power is defined below;

$$U_T = \frac{\int F_x dx + \int F_y dx + \int F_z dx}{V} \quad \text{i}$$

Where U_T is the total power (N/mm^2), $F_{x,y,z}$ are the forces recorded by the dynamometer (N), x is the distance of the cut (mm) and V is the volume of material removed (mm^3).

2.3. Post machining assessment

2.3.1. Focus variation assessment

Areal surface scanning was conducted using an Alicona InfiniteFocus SL focus variation system using 10 x magnification. Exposure was set to 7.25 ms and contrast set to 0.7 with vertical resolution and lateral resolution set to 200 nm and 1 µm respectively. A scanning area of 5 x 3 mm (complete thickness of sample) was taken (see Figure 2 c)). A λ_c filter value of 0.8 mm was applied to the image before volumetric, spatial, bearing area and autocorrelation textural parameters were collected from Alicona IF-Measurement Suite software in accordance with ISO 25178 [41]. λ_c is the cut-off wavelength which determines the amount of waviness removed from the measurement to visualise high-spatial frequency roughness parameters.

As R_a is widely used within industry, a comparison between 2D to 3D data is necessary. In addition to more advanced parameter collection using areal techniques, R_a data was collected and measured to ISO 4288 [42] and ISO 3274 [43] specifications with a cut-off wavelength of 0.8 mm and a tip radius of 5 µm. It is known that taking measurements along the length of each ply of the laminate in the direction of cutting, i.e. along only 0, ±45 and 90° fibre directions produces very different surface roughness values [15]. Therefore five measurements were taken in the transverse fibre

direction across the full thickness of the specimen/transverse to the direction of cutting, incorporating all laminate fibre orientations as shown in Figure 2 c) for comparison to S_a values.

2.3.2.Scanning electron microscopy

A ThermoFisher Scientific FEI Inspect F SEM was used to assess damage at high magnification on the machined edge (see Figure 2 c)). Sputter gold-coated samples were mounted on 32 mm diameter stubs using Electrodag 1415 silver conducting adhesive (Agar Scientific, UK). A 5kV accelerometer voltage and a level 3 spot size were used to view the CFRP material.

2.4. Flexural testing

Four point static bending to ASTM D6272 [44] using one half support span was completed for all machined specimens using a Tinius Olsen H5K-T tensile/compression test rig to assess differences in mechanical performance. Four point bending was chosen based on previous successful attempts to link surfaces to mechanical performance [18, 19] whereby a large portion of the edge can be placed under loading conditions to exacerbate the edge condition which is due to machine and/or tool. A Tinius Olsen 500LC laser extensometer was used to determine mid-point deflection with one half, rather than one third, support span used to enable the maximum amount of machined surface to be 'active' and in shear. Flexural modulus was taken as an average of five gradients taken from the load-displacement curve. As per the specification, individual crosshead rates were used to account for minor dimensional differences between specimens. Flexural testing has also been chosen due to the small specimen size. It is known that robotic machining can have dimensional tolerance issues [33, 34] so by limiting the movement of the robot to a small area, large scale dimensional errors can be potentially avoided. Flexural strength values are also a function of specimen width and thickness so any small dimensional errors produced by robotic machining can be accounted for.

3. Results and discussion

3.1. Characterisation of manufactured panels

DSC results show that a 99.99 % cure was achieved using the given cure schedule. This indicates the stoichiometric mixing regime is correct and the DGEBF freely reacts with the TETA hardener without a need for additional post curing or chemical additions such as accelerators.

DMA analysis gives an average tan δ Tg of 115 °C for all four panels with a standard deviation of 0.63 °C which indicates that the panel manufacturing process is repeatable.

Optical microscopy shows that all panels have the correct number and orientation of plies. Table 4 shows the fibre, resin and void content for all manufactured panels. The void content for all panels is low (0.36 % average) which is indicative of the RTM process.

Overall it has been shown that the manufacturing process has minimised variables in such a way to improve panel consistency which reduces errors which could potentially provide misleading information during machining and post-processing.

3.2. Milling equipment

3.2.1.Static modal tap testing of machines

Figure 3 shows the frequency versus magnitude plot for the FTV and ABB machines at the point of initial tool engagement with the workpiece. There is a clear difference in machine stability inferred from the frequency response result shown in Figure 3. Practically this means that the FTV is more rigid than the ABB which is expected due to the 3 joints within the robotic system compared to the relatively stable overhead gantry about which the FTV machine moves.

3.2.2.Dynamometer

Performing an FFT to dynamometer data showed that the correct speed of 14,400 RPM was achieved on both platforms. The cutting speed of 271 m/min was confirmed separately by observing raw dynamometer forces in the time domain. Figure 4 shows that the average U_T for the FTV is higher than the ABB machine.

This suggests that the tool is held more rigidly against the workpiece for the FTV therefore more energy can be transferred to the CFRP. This is in agreement with stability analysis that demonstrates the FTV enables a more rigid setup than the ABB machine. The graph also shows that U_T for the DIA-HBC4 tool is higher than the DIA-BNC tool. This fits with the feed per tooth (FPT) values of the tools used where the DIA-HBC4 tool FPT is double the DIA-BNC tool.

In order to establish the significance of measured parameters to factorial responses of machine and tool, Minitab has been used to analyse the factorial design against various parameters. In order to understand the importance of each variable (U_T, S_a, S_q etc.) to the response (machine, tool, machine-tool) further analysis has been completed by creating Pareto plots, highlighting the relative importance of each response if a relationship to the variable is present. The Pareto classification of each variable with respect to machine and tool factors is given in terms of primary, secondary and tertiary relationship.

The ANOVA for UT with respect to machine, tool and machine-tool interactions is shown in Table 5. This shows that there is a statistical link between both machine and tool to UT where machine has the primary Pareto effect. This is in agreement with Figure 4 and the above discussions.

3.3. Post machining assessment

3.3.1.Focus variation assessment results

Figure 5 shows depth profiles obtained through focus variation and the sections of tools used to cut specimens for each machine. It can be seen that the tools impart their geometries onto the surfaces of the CFRP specimens. The DIA-HBC4 tool presents an obvious herringbone pattern on the machined surface with an intersection where the two opposing helixes meet. The DIA-BNC tool shows bands of teeth which are present only in the ABB machine. This suggests that the reduced stiffness of the robotic process not only in the x/y plane but also in z which results in a greater opportunity for non-linear trocoidal motion in the tool path. Whilst the stiffness of the robot is known to be highly transient when reaching larger points in the working envelope, this result suggests that even minor positional changes result in a degree of flexibility.

As well as imparting the tool geometry on the surface of the CFRP, the images show the underlying fibre structure in particular the -45° orientation which is due to the chip formation mechanisms involved in machining this fibre orientation which manifests as fibre pull-out seen as low areas coloured blue in Figure 5.

Complete ANOVA results for focus variation assessments are given in Table 6. When considering statistical links between variable and DOE factors, only the S_{al} autocorrelation metric is able to statistically determine surface differences due to the machine (p-value = 0.007). S_{tdi} (texture direction index) is also able to statistically show differences between machines however this is a tertiary Pareto effect and the tool has greater effect on the S_{tdi} parameter (p-value = 0.014). The S_{tdi} metric also shows tool and machine-tool factors have larger effects (p-value < 0.001 and 0.007 respectively).

As machine is the main contributor to the total power of the edge cut, U_T, the S_{al} metric may be able to identify changes in total power. As S_{al} is a metric which is more biased towards waviness changes than smaller scale roughness, it is able to show the difference in the machine stability (presented in Figure 3). A higher S_{al} value means that the surface is dominated by low frequency, long wavelength components whereas for a lower S_{al} value, the opposite is true (high frequency, low

wavelength). The FTV has a higher mean S_{al} value than the ABB (72.50 versus 65.33 µm, respectively) meaning that the stiffer FTV 5-axis elevated gantry milling machine generates a lower frequency, longer wavelength topography structure compared to the 6-axis articulated robotic ABB system, a difference which is statistically significant between the two machines (p-value = 0.007 as per Table 6).

ANOVA results for the machine response also show that S_a, a widely used parameter, is not a statistically significant (p-value = 0.928). This 3D metric analysis is in agreement with Slamani, Gauthier and Chatelain [35] who note that the 2D measurement, R_a, is not different between the two machines used in their study. The cutting tool and machine-tool combination are statistically significant with p-values of 0.004 and < 0.001 respectively. Whilst there is a stability difference between the two machines, S_a is not able to differentiate between samples cut by the two machines.

When visually examined, each tool imparts a different topography (see Figure 5). The results in Table 6 confirm that this geometry difference is recognised only by S_a, S_q, S_p, S_v, S_z, S_{10z}, S_{sk}, S_{dq}, S_{dr}, S_{tr}, S_{tdi}, S_{vk}, S_{mr1}, S_{mr2}, V_{vv} and V_{vc}/V_{mc} parameters (p-value < 0.05).

In addition to using ANOVA to attain links between the measured surface metrics and the DOE factors (Table 5 and Table 6), linear regression analysis has been completed to provide links between U_T and flexural strength responses to measured surface metric variables (Table 7) where machine and tool groups are combined.

Table 7 shows that for U_T, the surface metrics S_z, S_{sk}, S_{ku}, S_{al}, S_{pk}, S_{mr1}, V_{mp} and V_{vc}/V_{mc} have p-values < 0.05, showing a statistical link between the total power generated and the given surface metrics. S_z, an extreme parameter that notes the average of the five highest peaks and five lowest valleys, decreases as total power increases. This suggests that there are less extreme peaks and valleys on the machined surface as power increases. S_{ku}, the Kurtosis, also decreases with an increase in power suggesting less sharpness in the overall peaks and valleys of the surface topography. The S_z and S_{ku} responses are shown in Figure 6. All other responses increase as power, U_T, increases.

An analysis of 2D versus 3D parameters for ABB machined coupons elucidated that the 2D parameters show the same trend as the 3D parameters, for example the DIA-BNC tool provides a rougher surface with a higher S_a and R_a than the DIA-HBC4 tool. It is noted that 3D parameters give larger values than the 2D counterparts (Table 8) which is expected due to the increase in measured -

45° fibres which have a chip formation method that leaves very rough surfaces. A traditional stylus would not be able to capture the full amount of damage present due to its limited tip size and the direction of measurement which could potentially fail to capture the roughness in -45° fibres. S_a and S_q give similar results to R_a and R_q whilst other amplitidue parameters, S_{10z}, S_p and S_v give much larger differences (from 142 to 208 % increases) indicating a higher sensitivity to spatial features such as sections of removed fibre. As the 3D parameters take into account the full specimen thickness across a 5 mm width and the 2D evaluation is taken from an average of five readings taken normal to the fibre direction across the full thickness of the specimen, the data demonstrates that the 3D value is more representative of the surface and the 2D measurements underestimate the surface roughness which aligns with findings of previous literature by Duboust *et. al.* [15].

If S_a were to be widely adopted by industry as a replacement for R_a, the acceptable limit should be increased by a certain factor. For example the acceptable R_a limit of a trimmed surface given by Montoya, Calamaz, Gehin and Girot [14] is 3.2 µm. In order to have a suitable S_a equivalent, the R_a value should be increased by 16 % (the average increase between the two tools from Table 8) to 3.71 µm. Only the FTV machine with the DIA-HBC4 tool would be able to meet this new S_a criterion with all other machine tool combinations above the 3.71 µm limit using the 271 m/min cutting speed of this experiment. This highlights the importance of following manufacturer's guidelines with the recommended cutting speed of 100-180 m/min likely to yield a much lower S_a value within acceptable limits.

3.3.2.Scanning electron microscopy results

Figure 7 shows a comparison of the specimens with the highest S_a value from each cutting tool and machine sample set for half the specimen thickness along its midline.

As noted previously in Figure 5, the ply orientation with respect to the cutting edge has a significant effect on the surface structure. Whilst the global view is in line with expected surfaces from literature sources [27-29, 40, 45] there is significant matrix smearing across all fibre orientations as shown in Figure 8 with the exception of -45° plies. In accordance with Sheikh-Ahmed [40] the cutting mechanics can be conveniently grouped as Type I, III, IV and V chip formation methods for different ply orientations. Type I chip formation describes 0° fibre cut through crack propagation ahead of the tool where the peeled layer then bends and fractures. This can be seen as some fibres have been bent and not fully snapped or held in place with resin as shown in Figure 8. The fibre tows also show

signs of matrix de-bonding where the matrix has been removed from around the fibre bundles. Type III and IV chip formation for 45° and 90° fibres respectively occurs through compression induced shear across the axis of the fibres followed by interlaminar shear fracture along the fibre matrix interface. Figure 8 shows that the matrix smearing is so significant that no fibres in the 90° orientation can be viewed. Whilst matrix smearing has occurred for the 45° fibre orientations, the underlying rough surface created by the Type III chip formation appears to be present. Type V chip formation mechanism occurs through macro-fracture ahead of the tool for -45° orientated fibres. Compressive stresses ahead of the cutting tool edge cause fibres and matrix to crack and form a long discontinuous chip. Type V chip formation causes the largest surface defects which can be seen in both Figure 7 and Figure 8. These images support existing theory [27-29] that notes that whole tows instead of individual fibres are bent and removed. The existence of the pull-out in the -45° direction accounts for the increase in 3D parameters compared to 2D parameters given in Table 4. S_{mr1} and R_{mr1} (which account for the fraction of surface that consists of peaks above the core material) are the exception to this where the change from 2D to 3D results in a decreased value suggesting that less peaks are above the core material. This can be explained by an increase in available data and therefore the S_{mr1} value is more realistic.

Matrix smearing is evident in all but -45° plies for all machine and tool combinations which suggests that the thermoset epoxy Tg is exceeded during continuous tool contact. This is highly significant as smearing may mask potential sub-surface defects, an observation also made by Kerrigan and O'Donnell [37]. This is also likely as the Tg of the DGEBF/TETA measured by DMA was noted as 115 °C, a temperature which is likely to have been exceeded during machining. The need for subsurface inspection is therefore critical and may offer an explanation to differing flexural strengths; given that the U_T is different between two machines this may have created differing levels of sub-surface defects which are then hidden from view.

3.4. Flexural Testing Results

Figure 9 shows the results of flexural testing between the machine and tool DOE variables. Through ANOVA, it can be seen that flexural strength varies between machines which, as noted in Table 9, has a statistically significant relationship (p-value < 0.001). Whilst there are some minor differences due to tools, DOE analysis has shown this to be statistically non-correlated (p-value of > 0.05). Whilst there is no statistical link between flexural strength and tool, there is a link between

flexural strength and machine-tool interactions (p-value < 0.001) suggesting that tools do play a role in the flexural strength but the effect is only apparent in conjunction with machines of different rigidity.

Previously calculated ANOVA results in Table 5 show that the total power is statistically different for both machines (p-value < 0.001). The ABB shows a lower measured total power during cutting than the FTV which can be explained by the stiffness of the machines; the ABB has 3 mechanical joints, each with a degree of compliance, which absorb some of the forces instead of transferring to the workpiece. Due to the full immersion nature of the cutting completed, the compliance is likely to be in the direction of cutting due to support from the carbon fibre in the direction normal to cutting. This in turn produces surfaces which lead to higher flexural strengths than the FTV machine.

Figure 9 also shows that flexural modulus does not change for machines and tools which is an expected result as the stress and strain rates of the material remain the same during bending and it is only the onset of failure which changes for samples cut by different machines and to a lesser extent by different tools. The point of failure is different between samples from different machines and it is this difference that has been captured through focus variation methods.

Using the Birmingham 14 parameters defined by Blunt and Jiang [46] it can be seen that of the types of s-parameters (defined as being height amplitude and spacing based), only the amplitude parameters are statistically correlated to flexural strength. Spacing parameters, based on spatial properties, hybrid parameters, based on both amplitude and spatial properties and extreme properties based on highest peaks and depths as well as texture direction do not correlate to flexural strength. All sub types within v-parameters (defined as being a function of material void and volume within peak, core and valley zones) show statistical significance showing that the v-parameters offer a rich wealth of statistical information which correlates to flexural strength.

Further analysis through linear regression fitting to show correlation between flexural strength and UT is shown in Table 10. It can be seen that flexural strength and UT are statistically linked. By observing the results from Figure 4, it can be seen that the lower power of the ABB machine produces higher flexural results. Conversely, the high power experienced in the FTV machine produced specimens which exhibited lower flexural strength.

4. Conclusions

- The flexural strength of coupons machined on the robotic arm is up to 25.9% (147.5 MPa) greater than those machined on the elevated gantry (p-value < 0.001). ANOVA shows that the machine and machine-tool interactions are statistically significant (p-value < 0.001). Therefore it is proposed that the damping within the 3 joints of the robotic machine causes lower total power transfer, U_T, from the tool to workpiece than the overhead gantry which manifest in a differing surface topography where more power transfer adversely affects the flexural strength.
- The tool geometry does play a role in the total power of the machining process (p-value < 0.001) but it does not influence the flexural strength (p-value > 0.05) directly. However the machine-tool interaction was shown to be statistically significant (p-value < 0.001). The tool geometry does play a role in generating different surface metrics with S_a, S_q, S_p, S_v, S_z, S_{10z}, S_{sk}, S_{dq}, $S_{dr\%}$, S_{tr}, S_{tdi}, S_{vk}, S_{mr1}, S_{mr2}, V_{vv} and V_{vc}/V_{mc} metrics all reporting p-values < 0.05 where the response is surface metric and the variable is the burr and herringbone tool.
- A comparison of 2D and 3D surface parameters shows that 3D parameters follow the same trends as 2D parameters but report larger values due to the increased observation area. If S_a were to be widely adopted instead of R_a, the R_a value should be increased by 16 %.
- Total power during machining should be kept to a minimum where possible to improve flexural strength. Results show that an increase in total power corresponds to a lower flexural strength values. Practically this can be achieved by lowering feed and speed however there may be an lower limit which leads to a drop-off in flexural performance which has not yet been explored. The choice of machine is also an important factor for total power between tool and workpiece with the robotic system providing lower total power overall.
- Through use of a DOE where machine and tool are set as variables, S_{al} and S_{tdi} metrics were able to show the difference in surface topography due to the machine (p-value < 0.001 and < 0.05 respectively) with mean results suggesting that the robotic machine generates a higher frequency, lower wavelength topography structure compared to the robotic machine (72.50 versus 65.33 µm) which matches expectations as the robotic system was shown to be less stable through static modal tap testing.

- SEM analysis concludes that matrix smearing is present due to the low Tg of the material which may be obscuring defects as well as influencing focus variation results.

5. Further work

Whilst this study has shown that there is a link between flexural strength and surfaces generated through edge trimming using different machines and tools, further work is required to capture the failure mechanisms at the point of rupture which would allow the exact nature of the failure defect to be traced and ultimately provide a more detailed link between surface metrics and defects.

6. Acknowledgements

The authors would like to acknowledge the EPSRC Industrial Doctorate Centre in Machining Science (EP/L016257/1) for the funding of this work and to the OSG Corporation for the supply of tools. Thanks are also extended to the Knowledge Transfer Centre and Factory 2050 at the AMRC.

7. Bibliography

[1] Farries P, Eyers C. Aviation CO2 Emissions Abatement Potential from Technology Innovation. V1.2 ed: Qinetiq; 2008.
[2] Strategic Research & Innovation Agenda. Advisory Council for Aviation Research and Innovation in Europe (ACARE); 2012.
[3] Meeting the UK aviation target - options for reducing emissions to 2050. Committee on Climate Change; 2009.
[4] Towards a 50% more efficient road transport system by 2030. European Road Transport Research Advisory Council (ETRAC); 2010.
[5] 21st Century Truck Partnership Roadmap/Technical White Papers. US Department of Energy; 2006.
[6] Remes H, Korhonen E, Lehto P, Romanoff J, Niemelä A, Hiltunen P, et al. Influence of surface integrity on the fatigue strength of high-strength steels. Journal of Constructional Steel Research. 2013;89:21-9.
[7] Akyildiz HK, Livatyali H. Effects of machining parameters on fatigue behavior of machined threaded test specimens. Materials & Design. 2010;31(2):1015-22.
[8] Bhaumik SK, Sujata M, Venkataswamy MA. Fatigue failure of aircraft components. Engineering Failure Analysis. 2008;15(6):675-94.
[9] Li B, Shen Y, Hu W. Casting defects induced fatigue damage in aircraft frames of ZL205A aluminum alloy – A failure analysis. Materials & Design. 2011;32(5):2570-82.
[10] Findlay SJ, Harrison ND. Why aircraft fail. Materials Today. 2002;5(11):18-25.
[11] Shaw MC. Metal Cutting Principles. Second ed: Oxford University Press; 2005.
[12] Haddad M, Zitoune R, Bougherara H, Eyma F, Castanié B. Study of trimming damages of CFRP structures in function of the machining processes and their impact on the mechanical behavior. Composites Part B: Engineering. 2014;57:136-43.
[13] Palanikumar K. Analyzing surface quality in machined composites. In: Hocheng H, editor. Machining technology for composite materials: Woodhead Publishing; 2012.
[14] Montoya M, Calamaz M, Gehin D, Girot F. Evaluation of the performance of coated and uncoated carbide tools in drilling thick CFRP/aluminium alloy stacks. The International Journal of Advanced Manufacturing Technology. 2013;68(9):2111-20.

[15] Duboust NG, H.; Pinna, C.; Ayvar-Soberanis, S.; Collis, A.; Scaife, R.; Kerrigan, K.;. An optical method for measuring surface roughness of machined carbon fibre reinforced plastic composites. 2015.
[16] Ramsden JJ, Allen DM, Stephenson DJ, Alcock JR, Peggs GN, Fuller G, et al. The Design and Manufacture of Biomedical Surfaces. CIRP Annals - Manufacturing Technology. 2007;56(2):687-711.
[17] Jiang X, Scott PJ, Whitehouse DJ, Blunt L. Paradigm shifts in surface metrology. Part I. Historical philosophy. Proceedings of the Royal Society of London A: Mathematical, Physical and Engineering Sciences. 2007;463(2085):2049-70.
[18] Arola D, Ramula M. Machining-induced surface texture effects on the flexural properties of a graphite/epoxy laminate. Composites. 1994;25(8):822-34.
[19] Arola D, Ramulu M. Net-shape machining and the process-dependent failure of fiber-reinforced plastics under static loads. Journal of Composites Technology and Research. 1998;20(4):210-20.
[20] Haddad M, Zitoune R, Eyma F, Castanie B. Study of the surface defects and dust generated during trimming of CFRP: Influence of tool geometry, machining parameters and cutting speed range. Composites Part A: Applied Science and Manufacturing. 2014;66:142-54.
[21] Sheikh-Ahmad JU, N.; Cheraghi, H. Machining Damage in Edge Trimming of CFRP. Materials and Manufacturing Processes. 2012;27:802-8.
[22] Ghidossi P, El Mansori M, Pierron F. Edge machining effects on the failure of polymer matrix composite coupons. Composites Part A: Applied Science and Manufacturing. 2004;35(7–8):989-99.
[23] Ghidossi P, Mansori ME, Pierron F. Influence of specimen preparation by machining on the failure of polymer matrix off-axis tensile coupons. Composites Science and Technology. 2006;66(11–12):1857-72.
[24] Eriksen E. The Influence of Surface Roughness on the Mechanical Strength Properties of Machined Short-Fibre-Reinforced Thermoplastics. Composites Science and Technology. 2000;60:107-13.
[25] Colligan KR, M. The Effect of Edge Trimming On Composite Surface Plies. American Society of Mechanical Engineers. 1992;Manufacturing Review Vol. 5(4).
[26] Wang XM, Zhang LC. An experimental investigation into the orthogonal cutting of unidirectional fibre reinforced plastics. International Journal of Machine Tools and Manufacture. 2003;43(10):1015-22.
[27] Girot F, Lopez De Lacalle LN, Lamikiz A, Iliescu D, Gutierrez ME. Machinability Aspects of Polymer Matrix Composites. In: Davim JP, editor. Machining Composite Materials: ISTE Ltd and John Wiley & Sons Ltd.; 2010.
[28] Wang DHR, M.; Wern, C.W. Orthogonal Cutting Characteristics of Graphite/Epoxy Composite Material1992.
[29] Wang DH, Ramulu M, Arola D. Orthogonal cutting mechanisms of graphite/epoxy composite. Part II: multi-directional laminate. International Journal of Machine Tools and Manufacture. 1995;35(12):1639-48.
[30] Wang DH, Ramulu M, Arola D. Orthogonal cutting mechanisms of graphite/epoxy composite. Part I: unidirectional laminate. International Journal of Machine Tools and Manufacture. 1995;35(12):1623-38.
[31] König W, Wulf C, Graß P, Willerscheid H. Machining of Fibre Reinforced Plastics. CIRP Annals - Manufacturing Technology. 1985;34(2):537-48.
[32] Konig WG, P.; Heintze, A.; Okcuand, F.; Justen, S. New Developments in Drilling and Contouring Composites Containing Kevlar Aramid Fibers. Proceeding on Design and Use of Kevlar Aramid Fiber in Composite Structures. 1984:99-103.
[33] Slamani M, Bonev IA. Characterization and experimental evaluation of gear transmission errors in an industrial robot. Industrial Robot: the international journal of robotics research and application. 2013;40(5):441-9.
[34] Dumas C, Boudelier A, Caro S, Garnier S, Ritou M, Furet B. Développement d'une cellule robotisée de détourage des composites. Mécanique & Industries. 2011;12(6):487-94.

[35] Slamani M, Gauthier S, Chatelain J-F. Comparison of surface roughness quality obtained by high speed CNC trimming and high speed robotic trimming for CFRP laminate. Robotics and Computer-Integrated Manufacturing. 2016;42:63-72.
[36] Heslehurst RB. Defects and damage in composite materials and structures: Boca Raton : CRC Press, Taylor & Francis Group; 2014.
[37] Kerrigan K, O'Donnell GE. On the Relationship between Cutting Temperature and Workpiece Polymer Degradation During CFRP Edge Trimming. Procedia CIRP. 2016;55:170-5.
[38] Ashworth S, Rongong J, Wilson P, Meredith J. Mechanical and damping properties of resin transfer moulded jute-carbon hybrid composites. Composites Part B: Engineering. 2016;105:60-6.
[39] Corporation O. OSG Aerospace Solutions - Composite. Aerospace Solutions - Composite2014. p. 54.
[40] Sheikh-Ahmad J. Machining of polymer composites: Springer; 2008.
[41] BSI. Geometrical product specifications (GPS) — Surface texture: Areal Part 2: Terms, definitions and surface texture parameters. ISO 25178-2:2012.
[42] BSI. Geometric Product Specification (GPS) — Surface texture — Profile method: Rules and procedures for the assessment of surface texture. BS EN ISO 4288:1998.
[43] BSI. Geometric Product Specifications (GPS) — Surface texture: Profile method — Nominal characteristics of contact (stylus) instruments. BS EN ISO 3274:1998.
[44] ASTM. Standard Test Method for Flexural Properties of Unreinforced and Reinforced Plastics and Electrical Insulating Materials by Four-Point Bending. ASTM D6272:2010.
[45] Koplev A, Lystrup A, Vorm T. The cutting process, chips, and cutting forces in machining CFRP. Composites. 1983;14(4):371-6.
[46] Blunt L, Jiang X. 2 - Numerical Parameters for Characterisation of Topography. Advanced Techniques for Assessment Surface Topography. Oxford: Kogan Page Science; 2003. p. 17-41.
[47] (BSI) BSI. Geometrical Product Specification (GPS) - Surface Texture: Profile Method - Terms, Definitions and Surface Texture Parameters. British Standards; 1998.
[48] Stout KJ, Sullivan PJ, Dong WP, Mainsah E, Luo N, Mathia T, et al. The Development of Methods for the Characterization of Roughness in Three Dimensions. Luxembourg: Commission of the European communities; 1993.

8. Figure Captions

Figure 1 – Milling machines a) FTV 5-axis elevated gantry and b) ABB 6-axis articulated robotic system

Figure 2 – a) flexural sample resulting from full slot milling, b) coupon arrangement in the fixture with dynamometer and fixture layout and c) post slot milling inspection areas

Figure 3 – Frequency versus magnitude plot showing differences in machine stability

Figure 4 – Comparison of UT for machines and tools displaying mean value and ± 1 standard deviation error bars from a minimum of 8 samples per tool

Figure 5 – Tools and tool geometry corresponding to surface depth images for edge trimmed specimens a) ABB, DIA-BNC b) ABB, DIA-HBC4 c) FTV, DIA-BNC and d) FTV-HBC4

Figure 6 – Linear regression fitted plots of Ut versus Sz and Sku

Figure 7 – SEM micrographs for highest Sa samples from a) FTV, DIA-BNC b) FTV, DIA-HBC4 c) ABB, DIA-BNC and d) ABB, DIA-HBC4 machine and tool combinations

Figure 8 – High magnification micrographs of ply orientation defects typical of both ABB and FTV machines and DIA-BNC and DIA-HBC4 tools

Figure 9 – Comparison of flexural strength and flexural modulus for different machines and tools displaying mean value and ± 1 standard deviation error bar from a minimum of 8 samples per tool, per machine

9. Tables

Table 1 – Experimental design of experiment with low and high text levels

Factor	Low	High	Replicates*
Machine	FTV	ABB	8
Tool	DIA-BNC	DIA-HBC4	8

*9 used for ABB, DIA-HBC4 combination

Table 2 – Cutting parameters used in experiment

Tool	No. Teeth	Tool diameter (mm)	Cutting speed (m/min)	FPT (mm/tooth)	Feed per revolution (mm/rev)
DIA-BNC	8	6	271	0.0082	0.066
DIA-HBC4	4	6	271	0.0165	0.066

Table 3 – Tool parameters

Tool	Helix Direction	Helix Angle (°)	Relief Angle (°)	Rake Angle (°)
DIA-BNC	Right	15	18	8
DIA-HBC4	Right & Left	30	18	9

Table 4 – Laminate content

	Fibre Content (%)	Resin Content (%)	Void Content (%)
Panel 1	52.63	46.98	0.39
Panel 2	57.13	42.74	0.13
Panel 3	55.16	44.38	0.46
Panel 4	54.42	45.12	0.46

Table 5 – ANOVA p-value results and Pareto classification for UT with respect to machine and tool factors

Key
Significant (<0.05)
Primary Pareto effect
Secondary Pareto effect
Tertiary Pareto effect

	p-value from DOE ANOVA		
Parameter (*Variable*)	***Machine***	***Tool***	***Machine/Tool***
U_T	***<0.001***	***<0.001***	0.098

Table 6 – ANOVA p-value results and Pareto classification for surface metric variables with respect to machine and tool factors (key as per Table 5)

			p-value from DOE ANOVA		
Parameter Group	**Sub-Group**	**Parameter (*Variable*)**	***Machine***	***Tool***	***Machine/Tool***
S-Parameters (based on height and spacing)	Amplitude	S_a (µm)	0.928	***0.004***	***<0.001***
		S_q (µm)	0.575	***<0.001***	***<0.001***
		S_p (µm)	0.207	***0.007***	***0.001***
		S_v (µm)	0.052	***<0.001***	***0.001***
		S_z (µm)	***0.035***	***<0.001***	***<0.001***
		S_{10z} (µm)	0.085	***<0.001***	***<0.001***
		S_{sk}	0.075	***<0.001***	***0.037***
		S_{ku}	0.231	***0.024***	***0.007***
	Hybrid	S_{dq}	0.244	***<0.001***	***0.008***
		S_{dr} (%)	0.390	***<0.001***	***0.006***
	Spacing	S_{al} (µm)	***0.007***	0.065	0.102
		S_{tr}	0.060	***0.006***	***0.029***
	Miscellaneous	S_{tdi}	***0.014***	***<0.001***	***0.007***
V-Parameters (based on Abbott-Firestone Curve)	Linear areal material ratio curve	S_k (µm)	0.817	0.133	***<0.001***
		S_{pk} (µm)	0.191	0.153	0.052
		S_{vk} (µm)	0.141	***<0.001***	0.060
		S_{mr1} (%)	0.084	***0.001***	0.794
		S_{mr2} (%)	0.778	***0.001***	0.056
	Material volume	V_{mp} (ml/m²)	0.212	0.287	***0.045***
		V_{mc} (ml/m²)	0.923	0.090	***<0.001***
	Void volume	V_{vc} (ml/m²)	0.628	0.896	***<0.001***
		V_{vv} (ml/m²)	0.229	***<0.001***	***0.033***
		V_{vc}/V_{mc}	0.110	***<0.001***	0.910

Table 7 - Linear regression p-value results for UT and flexural strength responses where surface metric parameters are variables

Key
Significant (<0.05)

			Regression P-value	
Parameter Group	**Sub-Group**	**Parameter (*Variable*)**	***U_T***	***Flexural Strength***
S-Parameters (based on height and spacing)	Amplitude	S_a (µm)	0.920	***0.015***
		S_q (µm)	0.583	0.059
		S_p (µm)	0.166	0.273
		S_v (µm)	0.060	0.701
		S_z (µm)	***0.046***	0.414
		S_{10z} (µm)	0.113	0.381
		S_{sk}	***0.004***	***0.023***
		S_{ku}	***0.015***	***0.006***
	Hybrid	S_{dq}	0.084	0.596
		S_{dr} (%)	0.130	0.504
	Spacing	S_{al} (µm)	***<0.001***	0.094
		S_{tr}	0.229	0.319
	Miscellaneous	S_{tdi}	0.060	0.238
V-Parameters (based on Abbott-Firestone Curve)	Linear areal material ratio curve	S_k (µm)	0.797	***0.02***
		S_{pk} (µm)	***0.023***	***0.005***
		S_{vk} (µm)	0.063	0.799
		S_{mr1} (%)	***0.005***	0.081
		S_{mr2} (%)	0.461	0.707
	Material volume	V_{mp} (ml/m²)	***0.027***	***0.004***
		V_{mc} (ml/m²)	0.634	***0.009***
	Void volume	V_{vc} (ml/m²)	0.316	***0.009***
		V_{vv} (ml/m²)	0.123	0.521
		V_{vo}/V_{mc}	***0.014***	0.15

Table 8 – 3D versus 2D parameter comparison (for all ABB samples)

Parameter		Increase from 2D to 3D (%)	
2D	**3D**	**DIA-BNC**	**DIA-HBC4**
R_a	S_a	**17**	**15**
R_q	S_q	**19**	**18**
R_t	S_{10z}	**142**	**156**
R_p	S_p	**208**	**172**
R_v	S_v	**154**	**201**
R_{sk}	S_{sk}	**39**	**74**
R_{ku}	S_{ku}	**59**	**74**
R_{dq}	S_{dq}	**48**	**50**
R_k	S_k	**31**	**24**
R_{pk}	S_{pk}	**15**	**15**
R_{vk}	S_{vk}	**15**	**14**
R_{mr1}	S_{mr1}	**-9**	**-13**
R_{mr2}	S_{mr2}	**2**	**1**

Table 9 - ANOVA p-value results and Pareto classification for flexural strength with respect to machine and tool factors (Key as per Table 5)

	p-value from DOE ANOVA		
Parameter (*Variable*)	***Machine***	***Tool***	***Machine/Tool***
Flexural strength	***<0.001***	0.700	***<0.001***

Table 10 – Linear regression p-value results for UT and flexural strength interactions (key as per Table 7)

	Regression P-value
Parameter (*Variable*)	U_T
Flexural Strength	***<0.001***

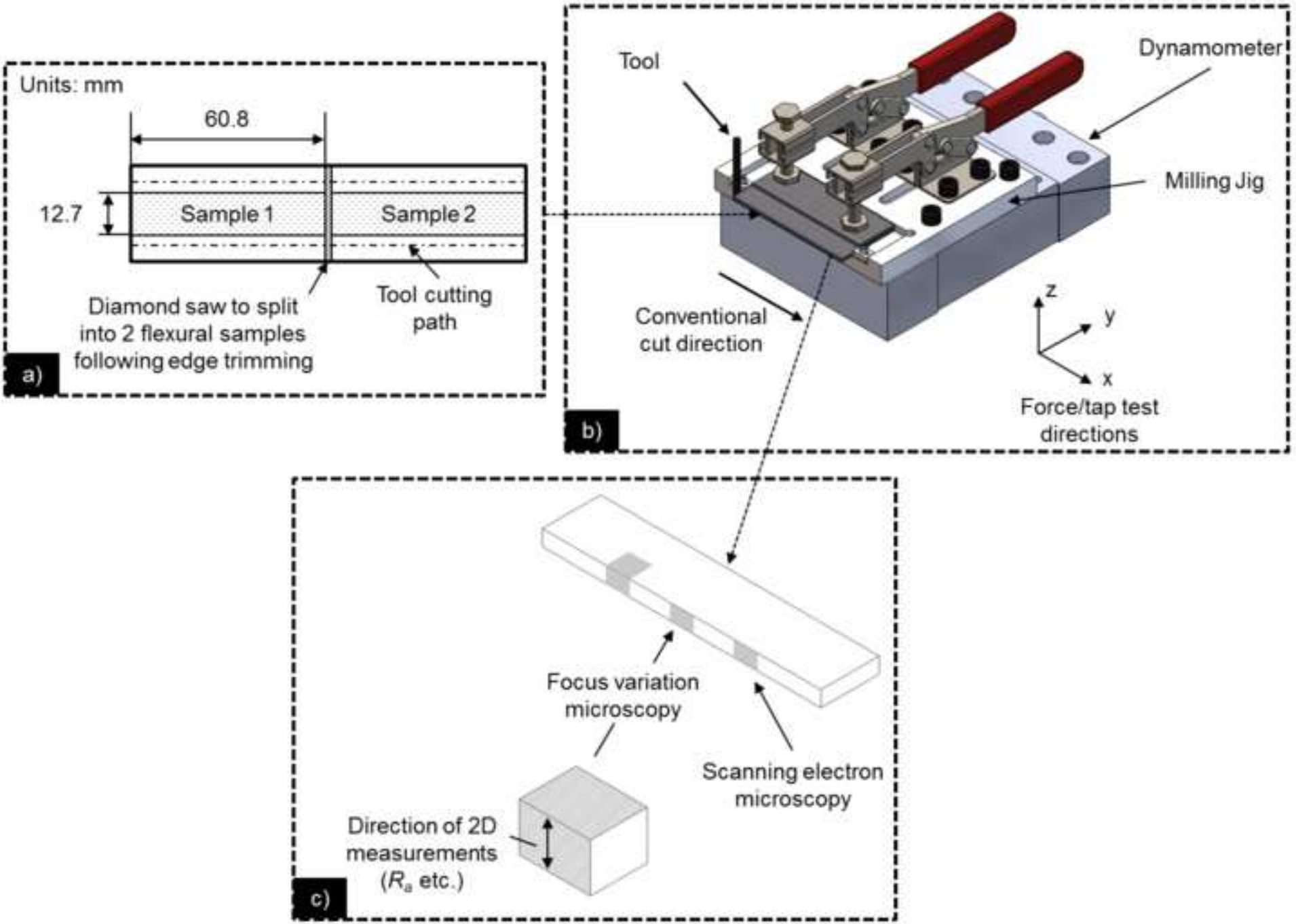

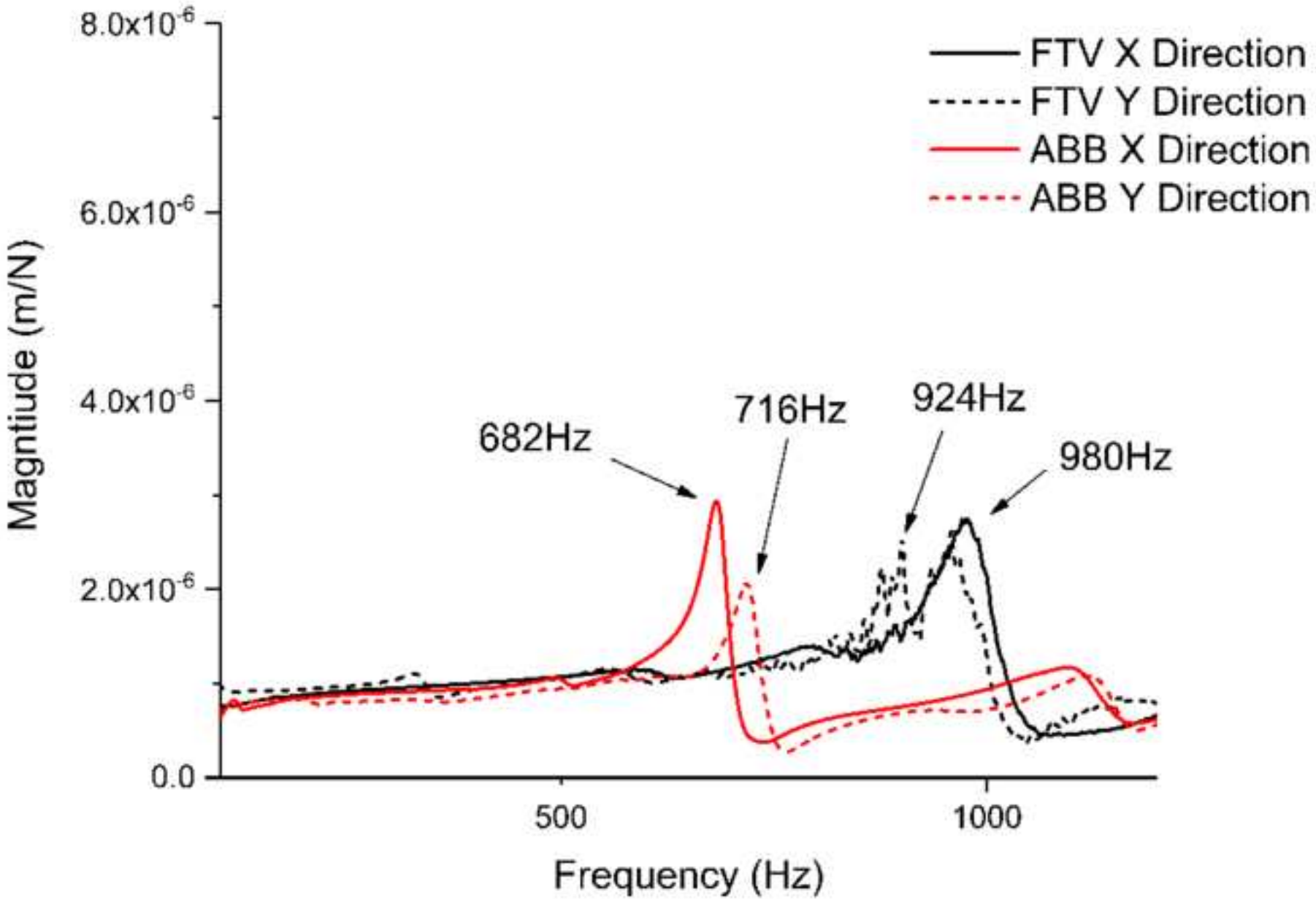
8.0x10-6
6.0x10-6
4.0x10-6
2.0x10-6
0.0
Magntiude (m/N)
500
1000
Frequency (Hz)
FTV X Direction
FTV Y Direction
ABB X Direction
ABB Y Direction
682Hz
716Hz
924Hz
980Hz